

The **De-Icing Comparison Experiment (D-ICE)**: A campaign for improving data retention of radiometric measurements under icing conditions in cold regions

*Science and Implementation Plan*

Christopher J Cox<sup>1,2</sup> and Sara Morris<sup>1,2</sup>

Project Leads

<sup>1</sup> Cooperative Institute for Research in Environmental Sciences (CIRES)

<sup>2</sup> NOAA Earth System Research Laboratory (ESRL) Physical Sciences Division (PSD)

July 31, 2017

## 1.1. Introduction and Problem Statement

Measurements of broadband shortwave (solar) and longwave (terrestrial) radiative fluxes at the Earth's surface are amongst the most fundamental environmental observations supporting process-understanding and forecasting at a range of time scales. The Baseline Surface Radiation Network (BSRN), under the auspices of the World Meteorological Organization (WMO), is the premier global network of such observations; the BSRN is traceable to a common calibration standard, managed using commonly adopted practices and is strategically distributed for global coverage. In the Arctic, NOAA has a vested interest in BSRN, operating three of the six BSRN stations north of the Arctic Circle and having in common with BSRN a core mission objective of maintaining long-term measurements in sparsely represented regions.

There are a number of environmental challenges in maintaining high-quality observations, some of which are specific to regional climates. In cold regions, including polar and alpine environs, and winter months at mid-latitudes, the build-up of ice on sensors results in large frequencies of compromised or lost data. The ice may be in the form of accumulation from snowfall, contact freezing from supercooled liquid droplets (rime) such as those in cold fogs, or from vapor deposition (frost) (e.g., Figure 1a). Since icing occurs under certain meteorological conditions, this loss of data in turn constitutes a climatological bias in the measurement records. Furthermore, post-processing of

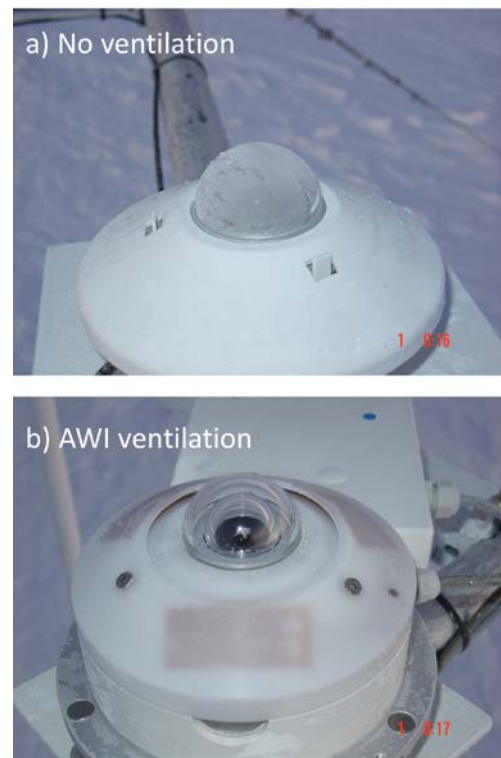


**Figure 1.** (a) Stock Kipp & Zonen CM11 with no ventilation at Georg von Neumayer station. (b) CM11 with ventilated housing designed by Alfred Wegener Institute (AWI). (photo credit: Gert König-Langlo).

data is hampered by the fact that the signal from data contaminated by icing is difficult to distinguish from the signal caused by clouds. The needs of the scientific community also increasingly require measurements of comparable quality to BSRN from stations capable of being autonomous for weeks or months at a time. Thus, an automated, low-power solution to the icing problem is sorely needed. In practice, this is a challenging goal because the nature of the measurement engenders sensitivities to thermal instabilities within the instruments, limiting the application of heat as an ice-mitigation technique. Recognition of the problem and mitigation attempts were reported during the earliest era of polar radiometric observations more than five decades ago (e.g., Koerner et al. 1963). Engineering solutions have been pursued by research institutes and industry, and while progress has been made, there is still no agreed-upon approach.

Manual cleaning of sensor domes is part of a daily operational maintenance of BSRN stations (McArthur 2005). Manual cleaning removes residues, films and dust and is also the recommended procedure for removal of ice. Unfortunately, the accretion rate of ice is much faster (minutes to hours) than can be reasonably maintained by manual cleaning (typically daily). Other proposed approaches for de-icing include automated wash systems (e.g., Persson and Semmer 2010), heated enclosures and various configurations of heating and/or ventilation. These approaches do not replace the need for daily maintenance, but if successful are likely to significantly increase the data retention rate.

During meetings held by the BSRN Cold Climates Issues Working Group (CCIWG) at BSRN Workshops in 2012 (Postdam), 2014 (Bologna), and 2016 (Canberra), experts have repeatedly identified ice-mitigation as a priority if the measurements are to be improved. Specifically, CCIWG has recommended that an effort be undertaken to test proposed solutions in

a comparison campaign with the objective of identifying an effective approach that does not adversely affect measurement uncertainty or that can be accounted for in post-processing.

## **1.2. Campaign Proposal**

Beginning April 2016, the new CCIWG lead is Christopher Cox (CIRES/NOAA-PSD). It was decided in the Canberra meeting that CCIWG would carry out a comparison campaign on the leading edge of the Year of Polar Prediction (YOPP) beginning in mid-2017. Cox and NOAA-PSD agreed to lead this effort.

Several BSRN stations affected by icing have reported increased data retention rates using ventilators, including the Sonnblick station in the Austrian Alps using a commercially available system (Weisser 2016) and the Georg von Neumayer station in Antarctica using a system designed by the Alfred Wegener Institute (AWI) (BSRN 2012). The AWI design relies on carefully directed airflow from a fan with no additional heating applied. The AWI experience has documented success in Antarctica (Figure 1). The DOE-ARM North Slope of Alaska Radiometer Campaign also reported that high-flow ventilation was a useful technique, but that ice mitigation was improved when the air was also heated (BSRN 2012). Several preliminary experiments have been conducted within NOAA-PSD, including at the Storm Peak Laboratory in Steamboat Springs, Colorado (Albee et al. 2015) and in Boulder, Colorado (Crepinsek 2016) that have yielded insight into the practicality of forced air using blowers and fans, the effectiveness of dome shape in shedding snow, and the adverse effects of heat.

Motivated by these efforts, NOAA-PSD in collaboration with NOAA-GMD and the CCIWG will carry out the De-Icing Comparison Experiment (D-ICE) in Barrow/Utqiagvik, Alaska, from August 2017 to August 2018. Following the emerging position of the BSRN

community that ventilation is a viable option, the guiding hypothesis for the experiment is that *ventilation of ambient air alone, if properly applied, is sufficient to maintain ice-free radiometers without increasing measurement uncertainty during icing conditions.*

This document outlines the experiment and implementation plans for D-ICE. We begin in Section 2 with a brief overview of the theory of operation for broadband radiometers and the magnitude of the effects of ice on the measurements. In Section 3 we describe the campaign setting and meteorological conditions that support riming at the campaign site, followed in Section 4 by the experimental design. Additional measurements are described in Section 5 and the data management plan is presented in Section 6.

## **2. Theory of Instrument Operation and the Scale of the Icing Problem**

At BSRN stations shortwave fluxes are typically measured with a thermopile pyranometer and longwave fluxes are typically measured with a thermopile pyrgeometer. These are essentially the same instrument. In both cases, the fluxes are inferred by measuring the voltage produced by a thermopile that is either warming or cooling from radiative gains and losses through the instrument dome, and relating the measured voltage to flux through a calibration procedure. The main difference between the instruments is in the domes that cover the thermopile, which are designed to isolate the target flux.

In a pyrgeometer, a single dome is used that is opaque to solar radiation so that the temperature differential across the thermopile is induced by longwave exchanges. Thus, the measured voltage corresponds to the net longwave flux ( $LW_{IN} - LW_{OUT}$ ) for the thermopile (for an upward facing instrument this is typically negative and measured as a negative voltage).  $LW_{IN}$

is then calculated by adding  $LW_{OUT}$  to the net, where  $LW_{OUT}$  is determined from a measurement of the thermopile case temperature, as follows:

$$LW_{IN} = \frac{V}{S} + \sigma T_c^4, \quad (1)$$

where  $T_c$  is the case temperature,  $\sigma$  is the Stefan-Boltzman constant (emissivity,  $\epsilon = 1$ ),  $V$  is the measured voltage and  $S$  is the calibration factor in  $Wm^{-2}/V$ . Eq. (2) assumes that the case, thermopile and dome all have the same temperature, but this is not necessarily true. Eppley pyrgeometers have a second thermistor to measure the dome temperature that is used to correct for differences in temperature between the case and dome. Applying the correction developed by Albrect and Cox (1977), Eq. (1) can be re-written:

$$LW_{IN} = \frac{V}{S} + \sigma[T_c^4 + D(T_c^4 - T_d^4)], \quad (2)$$

where  $V$ ,  $S$ ,  $T_c$  and  $\sigma$  are as before,  $T_d$  is the dome temperature and  $D$  is a pre-defined unit-less “dome correction factor”, taken nominally to be 3.5. For Kipp & Zonen pyrgeometers, the dome and case are designed to be in thermal equilibrium and Eq. (1) is used.

A pyranometer has paired domes transparent between approximately 0.3 and 2.8  $\mu m$  to transmit sunlight to the thermopile, while the paired configuration insulates the thermopile from infrared (longwave) loss. The voltage reading is positive (indicating warming of the thermopile by the sun) and the flux ( $SW_{IN}$ ) is calculated by the simple relationship:

$$SW_{IN} = \frac{V}{S}, \quad (3)$$

where  $V$  is the measured voltage and  $S$  is the calibration factor in  $Wm^{-2}/V$ . An important assumption is that any temperature gradient across the thermopile is caused by  $SW_{IN}$  and not

produced as a result of a temperature differential within the instrument. The thermopile is free to change temperature because of processes not associated with the direct absorption of sunlight, but these temperature changes must be uniform across the thermopile. However, because the pyranometer dome does not act as a perfect insulator, some infrared loss (IR-loss) from the top of the thermopile occurs, inducing a

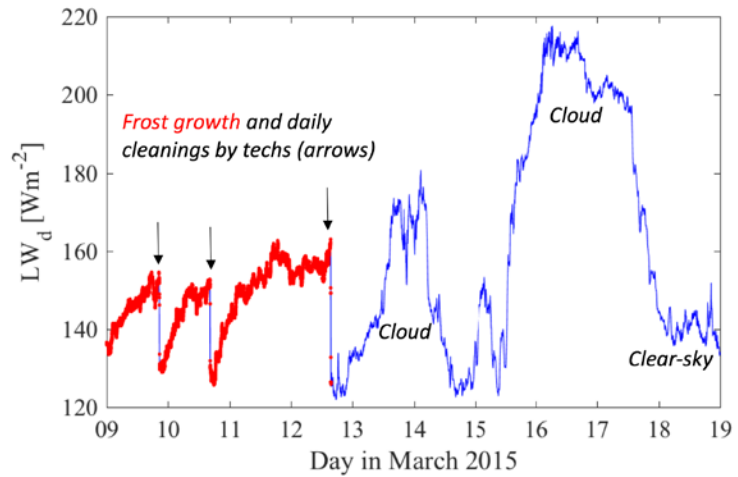


**Figure 2.** Frost growth curves (red) on downwelling longwave flux ( $\text{W m}^{-2}$ ) under cold, clear skies at Eureka in March 2015. As the frost grows, the measurement records more emission from the frost and less from the sky. The brightness temperature of the frost is greater than that of the sky and emits at frequencies where atmospheric gases are transparent, so an increase in flux is observed that abruptly disappears after cleaning (arrows). Observations made when the dome is contaminated by ice are within the temporal and magnitude range of the signal caused by clouds (e.g., on the 13<sup>th</sup> and 16<sup>th</sup>-17<sup>th</sup>), making the contaminated data difficult to distinguish in post-processing.

slight negative voltage offset and biasing the measurement low (Dutton et al. 2001 and references therein). During nighttime in Boulder, CO ( $\text{SZA} > 93^\circ$ ) when  $SW_{IN} = 0$ , the offset is observed to be  $-5$  to  $-15 \text{ Wm}^{-2}$  with the largest offsets occurring under clear skies (Dutton et al. 2001). The magnitude offset also varies between instruments.

Typically, pyranometers are ventilated to reduce the thermal gradients within the instrument and thus reduce the offset. Aspirating pyrgeometers are also common and recommended by BSRN (McArthur 2005) to reduce the magnitude of the correction factor in Eq. (2), in addition to being an acceptable means for reducing moisture and ice on the dome for both instrument types. Thus, the concept of ventilation is central to maintaining accurate observations even in the absence of icing, which makes ventilation an ideal ice-mitigation solution.

When ice builds on pyranometer domes, the measured signal can either increase (e.g., through refraction by the ice) or decrease (by reflection, refraction and/or absorption that prevents sunlight from reaching the thermopile). The influence can theoretically reach 100% loss of signal for a pyranometer completely covered in ice and snow, which may be 100's of  $W m^{-2}$ . When ice builds on pyrgeometer domes, emission from the ice itself is incorporated into the signal. Under clear skies ice will increase the longwave signal both because it is likely warmer than the sky and because it emits at frequencies where atmospheric gases do not. The magnitude of the bias imposed by the ice is dependent on the sky conditions, the temperature of the ice and the thickness and coverage of the ice on the dome. Figure 2 shows an example of (likely) frost on a pyrgeometer at Eureka, Canada, during a clear period, illustrating the similarity in magnitude and time scale to clouds that are also shown in the figure.

### **3. Campaign Setting and Meteorology**

D-ICE will be deployed at the NOAA Global Monitoring Division's (GMD) Barrow Atmospheric Baseline Observatory (71.3130°N, 156.6114°W, 11 masl), on the roof of the main facility (henceforth, "BRW") (Figure 2). The observatory is staffed year-round by two technicians and instrumentation receives daily maintenance. The BRW roof is the location of the Barrow BSRN tracker installation (beg. 1993) (green arrow in Figure 2), which includes ventilated (DC fan) and shaded downwelling longwave measurements (Eppley PIR) as well as diffuse (Eppley PSP), global (Eppley PSP) and direct (Eppley NIP) shortwave measurements. This BSRN station receives daily cleaning and logging of ice build-up, but does not include any special mechanical modifications for mitigating ice. BRW was selected as an ideal location for D-ICE because of the close partnership between BSRN, NOAA-PSD and NOAA-GMD, and also because Barrow is a

location representative of the types of conditions that are the target of D-ICE (discussed next) and logistics for Barrow deployment are relatively simple compared to other Arctic stations.

The main objectives of the experiment require analysis of nighttime data, although the nighttime data does not necessarily need to occur coincidentally with icing conditions. At Barrow, the sun sets for the polar night on November 18 and rises again on January 25. The autumn transition contains significantly less sunlight than the spring transition (SZA > 93° approximately 40% and 60% of the time in September and October, respectively, but only 24% in April and < 1% in May).

Barrow is situated on a point along the northern coast of the North Slope of Alaska, where

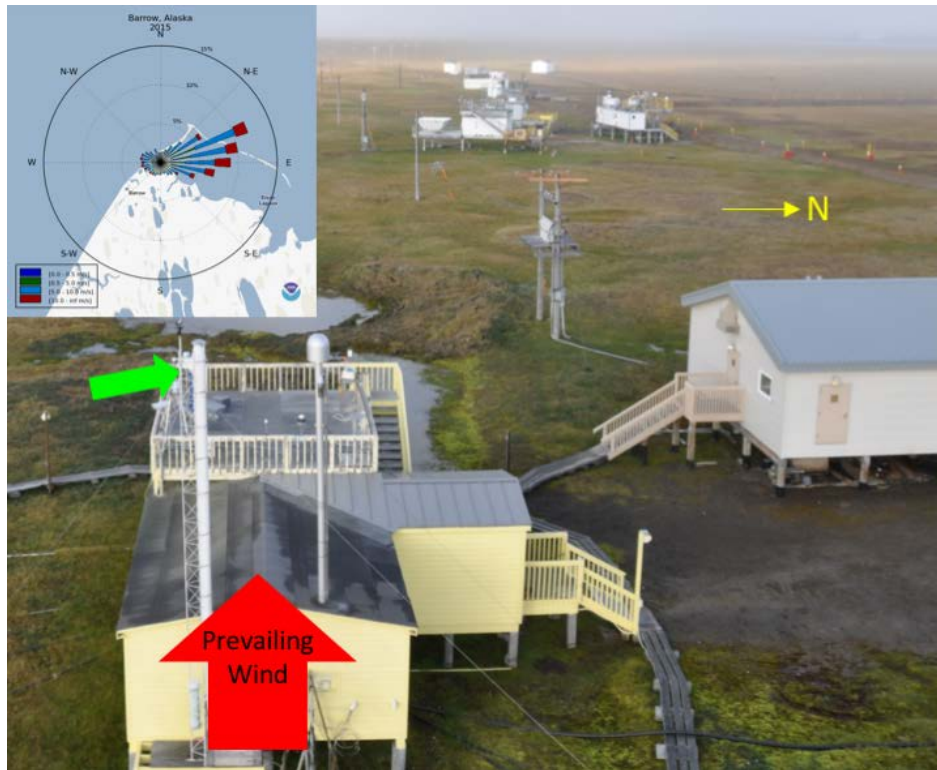


**Figure 3.** Image of the GMD Barrow facility facing west. Prevailing wind (red arrow) is approximately from the east-northeast (inset). The green arrow shows the location of the Barrow BSRN tracker on the facility roof where D-ICE will be deployed. Image an inset from <https://www.esrl.noaa.gov/gmd/obop/brw/>.

the prevailing winds are approximately east-northeast in all months, circulating around the Beaufort High and over a long fetch of ocean (Figure 3). The long-edge of the BRW building is

oriented approximately in line with the prevailing winds. The average two-meter air temperature is above freezing at Barrow only from June through September, while winter (DJFM) temperatures are typically between -20 and -30 C (Figure 4a). For the months of October through May, the near-surface air is close to saturation with respect to ice, indicating a propensity for icing conditions in these months (Figure 4b). The cloud fraction is high in all months and generally exceeds 90% from August through November (Figure 4c). The seasonal cycle in cloud fraction results in slightly less available sunlight during the autumn transition compared to the spring transition (Figure 4d). The peak in liquid-only cloud fraction and drizzle/rain is in August and these conditions are uncommon from October through April; liquid is present in the overwhelming majority of clouds in summer and autumn, but is only present in about half by spring (Shupe 2011).

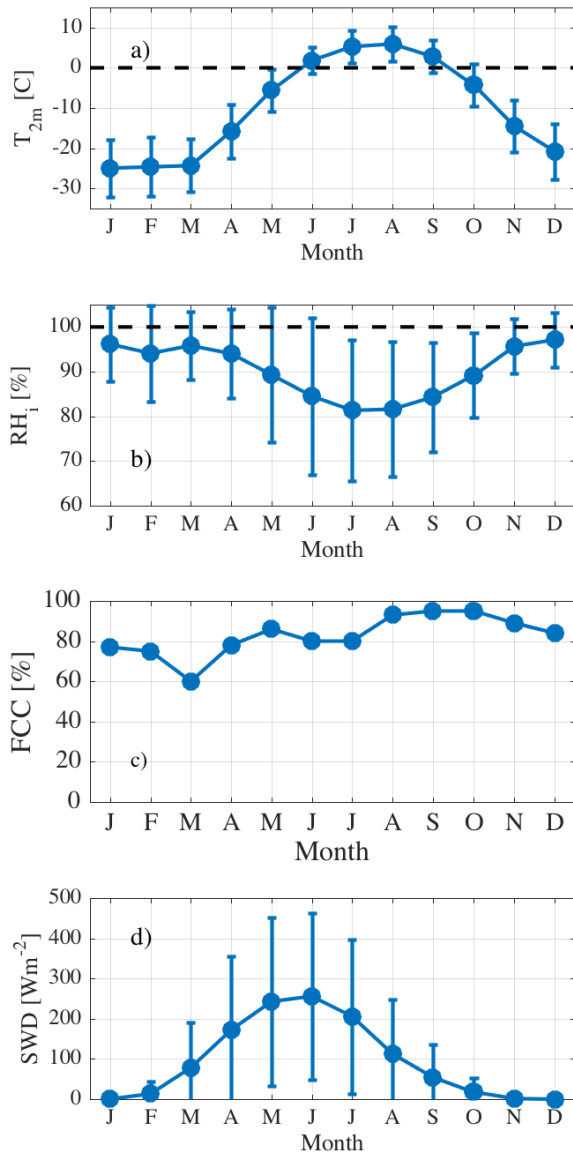


**Figure 4.** (a) Monthly mean  $\pm 1\sigma$  air temperature at 2m from Barrow (NOAA-GMD), 1993-2014. (b) as in (a), but relative humidity w.r.t. ice. (c) is fractional cloud cover (FCC) reported by Shupe et al. (2011). (d) as in (a), but for downwelling shortwave radiation.

The NOAA National Weather Service (NWS) operates a station at the Wiley Post/Will Rogers Memorial Airport, approximately 7 km southwest of BRW where daily weather observer reports are kept. Figure 5 shows the frequencies (percent of days in each month) when weather

conditions relevant for D-ICE were observed from 2000-2016. Fog (ice or liquid) is observed at least 70% of the time in all months and freezing fog is most common during transition months, occurring on 14-33% of days in April, May, June, October and November. May and October are the only two months when rime is observed on 10% or more of days. In addition to regular occurrences of snow and blowing snow, rain is common in the early autumn.

Figures 4 and 5 indicate that May and October are the two months when D-ICE is most likely to encounter the types of events that will provide the case studies needed. It is anticipated that 41.4 days between September 2017 and May 2018 will include conditions that may support riming, 14 of those days are expected to have significant riming with 5.3 significant riming days expected to occur in October 2017. Snow and drifting snow are expected to be common, occurring more than half of the time. Frost, which may be expected to occur predominantly under radiatively clear skies with high near-surface humidity with respect to ice is likely to be relatively common, occurring on 30-40% of days from December through March, which correspond to the months with relatively low cloud fraction and high occurrences of supersaturation with respect to ice.

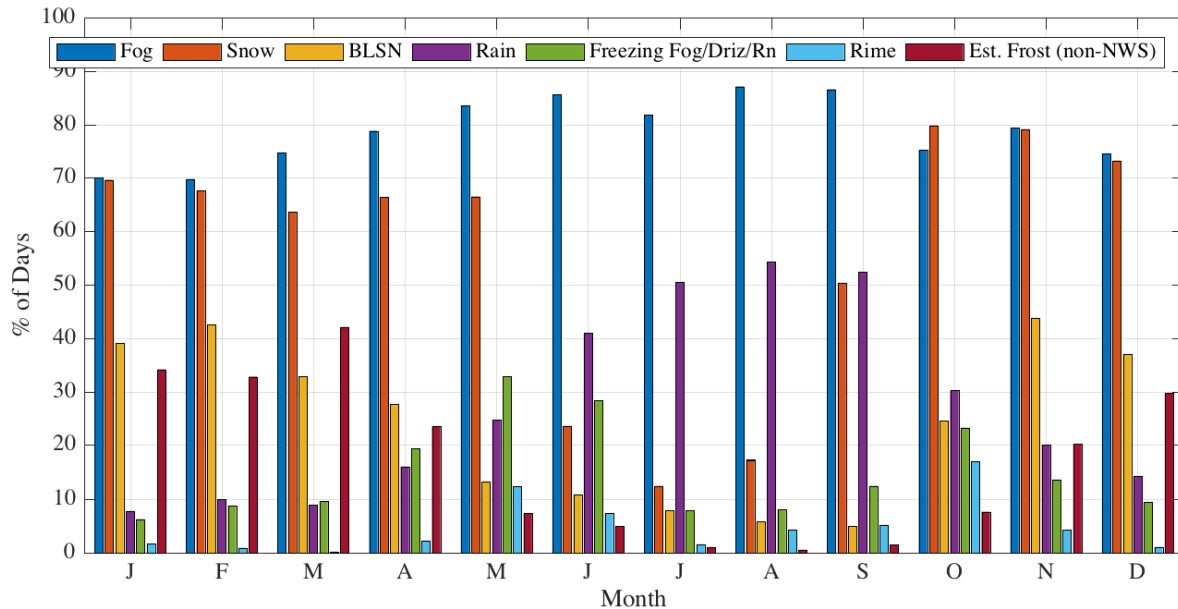


**Figure 5.** Frequency of days in each month (2000-2016) that National Weather Service observers at Barrow report any type of fog (dark blue); snow (light red); blowing snow (BLSN) (orange); rain (purple); freezing fog, freezing drizzle, ice fog, sleet or freezing rain (green); and rime (light blue). Dark red is a proxy for frost conditions based on finding the frequency of radiatively clear skies (longwave cloud radiative effect <math>< 20 \text{ W m}^{-2}</math>) and relative humidity with respect to ice > 95%.

#### 4. Experimental Design

The BSRN station at Barrow will serve as an independent measurement using the standard BSRN procedures. D-ICE will be installed adjacent to the BSRN station. The installation will be on fiberglass tables to electrically isolate the radiometers and housing units from one another. Two 8' x 1.4' tables will be constructed and set up end-to-end orthogonal to the prevailing winds so that the radiometers will not shield one another from wind or weather exposure. A schematic plan-view of the table design is represented in Figure 6.

##### 4.1. Radiometers and Calibration

Figure 6 also shows the layout of radiometers that will be tested. The primary radiometers are shown in blue (pyranometers/shortwave) and red (pyrgeometers/longwave) in the figure. All

radiometers will be tested facing upwards. Radiometers from the following companies are included: Delta-T, Hukseflux, EKO, Kipp & Zonen (KZ) and Eppley. Most radiometers in use at BSRN stations are either KZ or Eppley. Specific instrument models manufactured by Eppley that are in use at BSRN stations include the PSP pyranometer and the PIR pyrgeometer. KZ instrument models typically used include the CMP11, CMP21 or CMP22 pyranometers and CGR4 pyrgeometers. The primary difference between the KZ models is the reported accuracy, but there is no significant difference in design geometry or materials used. Both KZ and Eppley have requested that their newest models also be included in the D-ICE campaign (Eppley: SPP pyranometer, and KZ: SMP22 and SGR4); the S-series KZ are identical to their C-series counterparts but are digital rather than analogue, while the differences between the PSP and SPP are minimal, though the SPP does have a lower reported IR-loss bias.

All participating radiometers were calibrated simultaneously by NOAA-GMD in Boulder, Colorado in June 2017. Per GMD calibration procedure, the pyranometers were mounted outside facing the sky and were unventilated. The pyranometer calibration period lasted for approximately

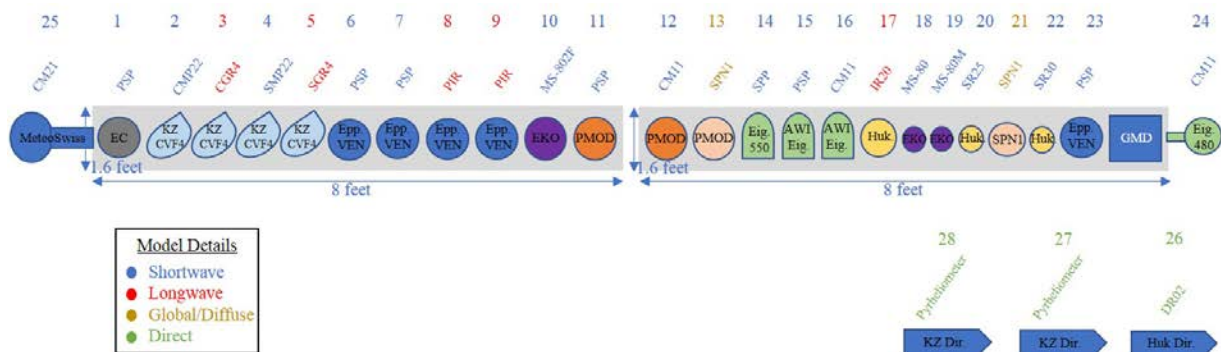


**Figure 6.** Schematic of the two D-ICE tables. The top row shows the model radiometer that will be housed in each of the ventilators represented to scale on the table; blue lettering for pyranometers/shortwave, red lettering for pyrgeometers/longwave. The following ventilation units will be tested: PMOD VHS ventilators (#11, 12, 13), Delta-T SPN-1 heated pyranometers (#13, 21), Hukseflux VU01 ventilator (#17), Kipp & Zonen CVP4 ventilators (#2-5), Eppley VEN ventilators (#6-9, 23), Eigenbrodt ventilators (#14-16, 24), MeteoSwiss ventilator (#25).

three weeks. The data collected from the calibration was saved and the data collected at night will be used to establish baseline IR-loss characteristics for each instrument involved.

## ***4.2. Ventilators***

Since ventilation is a primary modification being tested to mitigate rime/snow collection on the domes of radiometers, it is important to accurately describe the differences in ventilation units used throughout the experiment. Figure 6 shows the layout of the ventilators being used in the experiment. Figure 6 also shows which radiometers will be housed in each ventilation unit.

### *4.2.1. SPN-1 heated pyranometer*

The SPN-1 uses an internal heater to keep the instrument ice-free to -20 C. The SPN-1 reportedly worked well to mitigate ice during STORMVEX at Storm Peak Laboratory (Mace et al. 2010; Matsui et al. 2012) as long as the temperature was above -20 C (C. Long, personal communication). Thus, two SPN-1's will be used, one in its stock configuration and another in a modified PMOD housing (described below).

### *4.2.2. Hukseflux VU01*

Hukseflux radiometers have internal heating mechanisms (1.5 W for the SR25 and IR20; 2.3 W with internal fan and heater for SR30), but will also each be housed in Hukseflux VU01 heated ventilators. The VU01 uses a 7.8 W fan and will be configured for D-ICE with a 10 W heater. The VU01 can be operated with or without the heater running. The VU01 is rated to -40 C. All components are DC.

#### *4.2.3. Kipp & Zonen CVF4*

KZ radiometers will be housed in KZ CVF4 heated ventilators. The CVF4 uses a 5.5 W heater and a 5 W ventilator. All components are DC.

#### *4.2.4. Eppley VEN*

Eppley radiometers will be housed in Eppley VEN unheated ventilators using 80 CFM DC fans.

#### *4.2.5. AWI Ventilator*

The AWI ventilators are from the brand Eigenbrodt that include a traditional Eigenbrodt unit fit for an Eppley brand radiometer, while the other Eigenbrodt unit is minimally modified to direct air differently for the KZ brand radiometer. Both use a DC fan and are heated, however we will not be utilizing the heating option for these ventilator units (the heated Eigenbrodt units described below will include the heat component). The components are similar to the standard BSRN station, but the housing is configured to direct air around the case (without contacting the case) and over the dome such that the flow is laminar and directed towards the tip of the dome. All components are DC.

#### *4.2.6. WRMC/PMOD Ventilation and Heating System (VHS)*

The VHS combines a typical DC fan ventilation setup with a 7.8 W heat ring mounted above the case but within the airflow before it intersects the dome with the objective of heating the air before it passes over the dome but after it has passed the case. Included also is a modified

PMOD unit with a larger opening fit for an SPN-1 radiometer unit; the modified PMOD was configured in-house via NOAA-GMD. All components are DC.

#### *4.2.7. Eigenbrodt SBL*

The Eigenbrodt SBL 480 is designed for KZ and the SBL 550 for Eppley radiometers; the difference lies in the wiring and design features. The SBL uses a 1.6 W ventilator and 25 W heater. The SBL can be operated with or without the heater running. The SBL is in use at the high-elevation Sonnblick BSRN station in Austrian Alps. Sonnblick reports that the SBL improves data retention, but needed to be modified with extension tubes at the air inlet to prevent the fan from being clogged with snow and ice (Weisser 2016). It is expected that modifications following Sonnblick will be incorporated for D-ICE. All components are DC.

#### *4.2.8. MeteoSwiss Ventilator*

The MeteoSwiss ventilator is designed for a KZ pyranometer. It uses a ventilator and heater. The fan ventilator is accompanied by an elongated mesh tube to assist in decreasing the amount of snow accumulation to the fan unit. All components are DC.

### **4.3. Experiment**

During D-ICE, all radiometer/ventilator systems will be operated continuously in the configuration shown in Figure 6 and will be maintained using the standard BSRN procedures, including daily maintenance and cleaning. The configuration in Figure 6 emphasizes testing pyranometers over pyrgeometers. While icing affects both instrument types, quantifying measurement uncertainties associated with the operating configuration is more practical for

pyranometers collecting data at night because the measurement is expected to equal zero  $\text{Wm}^{-2}$  since there is no incoming solar radiation while the sun is below the horizon. It is anticipated that the results are transferrable to pyrgeometers when ventilation designs take into account the differences in geometry between pyranometer and pyrgeometer domes. Several pyrgeometers are included in the experiment in order to provide a limited test of this hypothesis. The campaign will begin collecting data in August 2017 and run through August 2018. The experiment will also be outfitted with visual data in the form of images captured from an optimally positioned outdoor camera. One camera will be placed at either end of the table to adequately capture whether or not ice/frost/etc. is accumulating on the domes of the radiometers. These images will assist in the final assessment to determine which ventilation unit best kept the radiometer domes clear throughout the annual cycle.

***Objective 1: Quantify the Impact of Icing on LW and SW Fluxes in the Arctic***

The first objective is to quantify the impact of icing on mean longwave and shortwave fluxes for a full annual cycle in the Arctic. Ice-mitigation will be compared to the following three controls: 1) compare against the standard operation of the collocated BSRN station on site, 2) compare against the standard operation of the nearby ARM station (< 1km away, will also be outfitted with a camera), and 3) and Eppley PSP and PIR will be situated in the standard Eppley VEN with DC ventilation, but will not be cleaned manually. In addition to these controls, visual data will also be collected to assess ventilation units that best keep the radiometer domes clean throughout the annual cycle (refer to Objective 2).

***Objective 2: Effectiveness of De-icing***

The second objective is to evaluate the effectiveness of each design in keeping the radiometer domes ice-free and to identify the conditions under which they are ineffective. With a full annual cycle record, it is anticipated that D-ICE will capture multiple events of rime, frost, blowing snow, rain, fog and precipitating snow (refer to Section 3). It is not possible to objectively and automatically determine the presence or amount of ice on the radiometer domes. Therefore, icing will be monitored using a low-light, cold-hardened security camera (1080 p) in a heated enclosure. The table will be illuminated using a floodlight, though the amount light will be minimized ( $< 1 \text{ W m}^{-2}$  at table level) to ensure that impact on the measurements is negligible. Images will be recorded every 15 minutes, generating a total of approximately 35,000 images over the course of the experiment. These images will be classified manually. A record will also be kept through the visual observations recorded by the technicians during their daily checks. Case studies will be examined and a statistical analysis of performance over the course of the campaign will be conducted.

### ***Objective 3: Impacts on measurement uncertainty***

The third objective is to quantify how the modifications change the uncertainty of the measurements. Isolating these effects from the atmospheric fluxes is best done by analyzing measurements made by pyranometers during night. When the solar zenith angle is  $> \sim 93$  degrees, the solar irradiance is negligible and a pyranometer will observe a value of  $0 \text{ Wm}^{-2} + \text{error}$ . Errors in pyranometers usually include a noise component and the negative offset described in Section 2 that is associated with IR-loss to the sky from the thermopile, which is not perfectly insulated. The characteristics of this radiative loss are dependent on the meteorological conditions (principally, temperature and cloud cover) and also on the temperature homogeneity and stability of the

instrument. Thus, poorly directed or weak aspiration, or differential heating will modify the behavior of the IR-loss. The IR-loss of the radiometers in their ventilated and heated housings will be compared to the base-state IR-loss characteristics that were quantified during the calibration period that took place in Colorado this June 2017. Comparisons will also be made to the collocated BSRN standard already located at the station, which will serve as the unmodified control. It is important that the influences of the ventilation and heating be quantified under the full range of temperatures and sky conditions observed, but it is not important that the influence be quantified specifically under icing conditions.

Case studies of IR-loss will be made under non-icing conditions under both cloudy and clear skies. For these cases the ventilators will be continually operated, while the heaters will be switched on and off for periods of time to compare the impact of heat to the system.

## **5. Ancillary Measurements**

To fully characterize the conditions that support icing and to properly classify the types of icing conditions that are encountered, additional atmospheric measurements are needed besides the flux measurements. Basic meteorological measurements are already collected at the Barrow station, but an additional Automatic Weather Station will be deployed on the BRW roof next to the D-ICE table. Specifically, the meteorological (MET) suite of instruments will contain a Lufft brand ultrasonic anemometer to capture wind speed and direction, an RTD temperature with Cambridge housing, a Vaisala HMP 155 relative humidity sensor, and a supercooled liquid water content (SLWC) sensor. The SLWC sensor exposes a sensor wire that vibrates with a fixed frequency. This frequency is impeded by the buildup of mass in the form of ice to determine supercooled liquid water content. It is yet to be determined if the SLWC sensor will be reliable

for the D-ICE application. The SLWC sensor can be used to calculate mass and accretion rate, but cannot distinguish the source of the icing. Additionally, atmospheric profiles using radiosondes are acquired every 6 hours in Barrow, at 0 and 12 UTC by the NWS site at the airport and at 6 and 18 Z by the U.S. Department of Energy (DOE) Atmospheric Radiation Measurement (ARM) program facility, location less than 1 km west of BRW. Also available from ARM is another independent broadband radiation station, as well as a suite of atmospheric remote sensors, including a cloud radar, lidar, microwave radiometer, ceilometer and spectral infrared radiances.

## **6. Data Management Plan**

Data from the D-ICE experiment will be collected using four Campbell Scientific CR1000 data loggers purchase by NOAA-PSD. The CR1000 data loggers will transmit data using a Digi-One SP serial to network adapter that will have a specific static IP address assigned to each one. Drivers for the Digi-One SP's will be installed on the data acquisition computer located at NOAA in Boulder, Colorado. The data acquisition computer will be located at NOAA-PSD where the camera and MET data will also be collected. Data will be collected daily and transferred to both the PSD and GMD servers internally so that data is visible in near real-time to the project leads. Images collected from the D-ICE camera system(s) will be pre-programmed to send images daily to an internal ftp location, and then redistributed to the DICE webpage. The cameras will also have microSD cards as a backup in the case that internet fails at the site and images cannot be immediately transferred per the schedule. All data and images will be publically available during the campaign on the DICE webpage that is hosted by NOAA-PSD. Data will be processed once the campaign has ended (August 2018) and published again on the PSD webpage or ftp site. The data will be processed using QA/QC techniques that be also described in detail at the conclusion

of the campaign. Data and images will be available throughout the campaign daily. Details outlining the specifics of the data management plan will be available on the DICE webpage.

## References

Albee, R., C. Cox, K. Knott, I. McCubbin and R. David, 2015: Proof of concept study with Albee Arctic Kick-ice System (AAKS) at Storm Peak Lab with results. Presentation at the Global Monitoring Division Annual Conference (GMAC), Boulder, Colorado, May 19, 2015.

Albrecht, B. and S.K. Cox, 1977: Procedures for improving pygeometer performance. *J. Appl. Meteorol.*, 16, 188-197, doi: 10.1175/1520-0450(1977)016<0190:PFIPP>2.0.CO;2.

BSRN, 2012: Report of the 12<sup>th</sup> Baseline Surface Radiation Network (BSRN) Scientific Review and Workshop, Potsdam, Germany, August 1-3, 2012. Available from:

[http://bsrn.awi.de/fileadmin/user\\_upload/bsrn.awi.de/Publications/BSRN-12-2012.pdf](http://bsrn.awi.de/fileadmin/user_upload/bsrn.awi.de/Publications/BSRN-12-2012.pdf)

Crepinsek, S. 2016: Radiometer rime/precipitation mitigation: Clear dome challenge. Report compiled for Independent Study, University of Colorado Department of Geography, Boulder, Colorado.

Dutton, E.G., J.J. Michalsky, T. Stoffel, B.W. Forgan, J. Hickey, D.W. Nelson, T.L. Alberta, and I. Reda, 2001: Measurement of broadband diffuse solar irradiance using current commercial

instrumentation with a correction for thermal offset errors. *J. Atmos. Ocean. Technol.*, 18, 297-314, doi: 10.1175/1520-0426(2001)018<0297:MOBDSI>2.0.CO;2.

Koerner, R. M. and coauthors, 1963: The Devon Island Expedition 1960-64. *Arctic* 16.1, 57-76.

Mace, J. and coauthors, 2010: STORMVEX: The Storm Peak Lab Cloud Property Validation Experiment Science and Operations Plan, ARM Technical Report, DOE/SC-ARM-10-021, ARM/Pacific Northwest National Laboratory, technical report, <https://www.arm.gov/publications/programdocs/doe-sc-arm-10-021.pdf?id=73>

Matsui, N., C.N. Long, J. Augustine, D. Halliwell, T. Uttal, D. Longenecker, O. Niebergall, J. Wendell and R. Albee, 2012: Evaluation of Arctic broadband surface radiation measurements. *Atmos. Meas. Tech.*, 5, 1-10, doi: 10.5194/amt-5-1-2012.

Persson, P.O.G. and S. Semmer, 2010: Impact of riming on Arctic surface energy budget measurements. Presentation at the Autonomous Polar Observing Systems Workshop, Potomac, Maryland, Sept 30-Oct 1, 2010.

Shupe, M.D., 2011: Clouds at Arctic Observatories. Part II: Thermodynamic Phase Characteristics. *J. Appl. Meteorol. Clim.*, 50, 645-661, doi: 10.1175/2010JAMC2468.1.

Shupe, M.D., V.P. Walden, E. Eloranta, T. Uttal, J.R. Campbell, S.M. Starkweather and M. Shiobara, 2011: Clouds at Arctic Observatories. Part I: Occurrence and Macrophysical Properties. *J. Appl. Meteorol. Clim.*, 50, 626-644, doi: 10.1175/2010JAMC2467.1.

Weisser, U., 2016: Status update of BSRN station Sonnblick (SON) – (Apr 2016). Presentation of the 14<sup>th</sup> BSRN Science Review and Workshop, Canberra, Australia, April 26-29, 2016.

Available from:

[https://www.esrl.noaa.gov/gmd/grad/meetings/BSRN\\_talks/P1\\_7\\_Poster\\_BSRN\\_Canberra\\_Olefs\\_Weiser\\_2016.pdf](https://www.esrl.noaa.gov/gmd/grad/meetings/BSRN_talks/P1_7_Poster_BSRN_Canberra_Olefs_Weiser_2016.pdf)

## Appendices

### *Appendix A: D-ICE Implementation Schedule*

<b>Task</b>	<b>Personnel</b>	<b>Due Date</b>
Rad daily cleaning schedule during calibration	Sara, Emiel, Chris	6/5 - 6/30
Send new d-ice programs to loggers for calibration	Jim	6/5
Level rads on NOAA roof so calibration can begin	Sara, Emiel	6/5
Transfer appended calibration file to PSD server (daily)	Sara, Elena	6/6
Check mV outputs from radiometers look realistic for calibration	Jim, Emiel	6/6
Drill out pilot holes for ventilator mounts	Sara, Emiel, Meghan	6/7
Plot daily mV outputs from radiometers during calibration	Elena	6/8

Position ventilator units on mounts; re-organize table layout	Sara	6/8
Secure mounts to fiberglass grate/table	Sara, Meghan, Nick	6/8
Build table (attach legs, frame, etc.)	Sara, Meghan, Nick	6/9
Figure out how logger boxes will mount to table side panels	Sara, Chris	6/9
Connect swiveling level feet and brackets to legs of table to stabilize it	Sara, Chris	6/23
Connector ventilators and heaters to system	Chris	6/23
Get SR30, and DR02 Hukseflux instruments connected	Chris	6/23
Figure out how to provide/shine light for cameras at Barrow (troubleshoot to see how radiometers are impacted by 100W lights)	Chuck, Taneil	6/23
Purchase lights for camera illumination	Chris, Taneil	6/23
Check that cameras work and collect data	Chris, Sara	6/28
Create D-ICE PSD ftp location & automated data transfer	Sara	6/28
Connect logger boxes and instruments to fiberglass table	Sara, Chris	6/29
Lock-tight all washers for the mounts once in right location on the table	Sara, Chris	6/29
Get computer system setup to receive data from Barrow	Sara	6/29
Purchase UPS for D-ICE local computer, purchase microSD cards for cameras	Sara	6/30
Test computer system/data transfer from loggers to computer	Sara, Jim	6/30
Create shipping documentation	Sara	7/3
Start packing up D-ICE system	Sara, Chris, Meghan	7/5
<b>Ship D-ICE system to Barrow</b>	<b>Sara, Chris, Emiel, Jim</b>	<b>7/6</b>
Finalize D-ICE data management plan for NCEI archive	Sara	7/7
Finalize D-ICE "datagram" documentation of full system/layout	Sara	7/7
Calibrate radiometers	Emiel	7/7
Finish D-ICE website	Sara	7/7
Develop automated D-ICE data plots	Elena	7/7
<b>Travel to Barrow to setup D-ICE</b>	<b>Sara, Chris, Emiel, Johan, Meghan, Nick</b>	<b>8/7 - 8/18</b>

### *Appendix B: D-ICE Contribution List*

Base Manufacturer	Base Model	Meas. Component	(Mod.) Source
<b>Radiometer Contributions</b>			
Delta-T	SPN-1	Shortwave	Delta-T
Delta-T	SPN-1	Shortwave	GMD - C.Long
Kipp & Zonen	CM21	Shortwave	Laurent Vuilleumier
Hukseflux	IR20	Longwave	Hukseflux
Hukseflux	SR25	Shortwave	Hukseflux
Hukseflux	SR30	Shortwave	Hukseflux
Hukseflux	DR04	DIRECT	Hukseflux
Kipp & Zonen	CMP22	Shortwave	Kipp & Zonen
Kipp & Zonen	SMP22	Shortwave	Kipp & Zonen
Kipp & Zonen	CGR4	Longwave	Kipp & Zonen
Kipp & Zonen	SGR4	Longwave	Kipp & Zonen
Kipp & Zonen	Pyrheliometer	DIRECT	Kipp & Zonen
Kipp & Zonen	Pyrheliometer	DIRECT	Kipp & Zonen
Eppley	SPP	Shortwave	Eppley



1	1	7	34231F3	ALERT	Shortwave	Eppley	PSP	8.41	EC, Alert
1	2	6	160478	171842	Shortwave	Kipp&Zonen	CMP22	9.74	Kipp&Zonen
1	3	6	160183	171840	Longwave	Kipp&Zonen	CGR4	9.4	Kipp&Zonen
1	4	6	160002	171843	Shortwave	Kipp&Zonen	SMP22	10.07	Kipp&Zonen
1	5	6	160008	171841	Longwave	Kipp&Zonen	SGR4	11.03	Kipp&Zonen
1	6	7	26818F3	V6-808	Shortwave	Eppley	PSP	8.57	Eppley
1	7	7	18135F3	V6-809	Shortwave	Eppley	PSP	8.65	Eppley
1	8	5	34309F3	V6 910-12	Longwave	Eppley, PSD	PIR	3.54	Eppley
1	9	5	28507F3	V6 909-12	Longwave	Eppley	PIR	3.76	Eppley
1	10	4	F16305R	MS-401FU	Shortwave	EKO	MS-802F	7.01	EKO
1	11	7	20523F3	PMOD	Shortwave	Eppley	PSP	9.67	PMOD
2	12	6	130814	PMOD	Shortwave	Kipp&Zonen, GMD	CM11	8.31	PMOD
2	13	5	A1571	GMD PMOD	Total, Diffuse	Delta-T, GMD	SPN		GMD, PMOD
2	14	7	38172F3	0932153	Shortwave	Eppley	SPP	8.05	Eigenbrodt
2	15	7	26236	0931190	Shortwave	Eppley, NCAR	PSP	9.07	Eigenbrodt
2	16	6	130819	0932088	Shortwave	Kipp&Zonen, GMD	CM11	8.7	Eigenbrodt
2	17	4	4037	Huk. Ven.	Longwave	Hukseflux	IR20-T1	10.13	Hukseflux
2	18	4	S16088025	MS80	Shortwave	EKO	MS-80	10.64	EKO
2	19	6	S16090016	MS80M	Shortwave	EKO	MS-80M	10.76	EKO
2	20	4	2510	none	Shortwave	Hukseflux	SR25-T1	14.87	none
2	21	4	A1338	none	Total, Diffuse	Delta-T	SPN		none
2	22	6	2060	none	Shortwave	Hukseflux	SR30-D1	10.29	none
2	23	7	26214	V6-689	Shortwave	Eppley, NCAR	PSP	8.52	Eppley, lift shield
2	24	6	130617	0932152	Shortwave	Kipp&Zonen, GMD	CM11	8.79	Eigenbrodt
2	25	5	970426	METEO SWISS	Shortwave	Meteo-Swiss	CM21	19.74	METEOSWISS
Tracker	Tracker, 26	6	9297	none	Direct	Hukseflux	DR02-T1-10	16.5	none
		7	26226	NCAR SPRAY	Shortwave	Eppley, NCAR	PSP	8.46	none, NCAR spray system
Tracker	Tracker, 27		999991		Direct	Kipp&Zonen	pyrheliometer	7.25	
Tracker	Tracker, 28		999992		Direct	Kipp&Zonen	pyrheliometer	7.52	

## ***Appendix D: D-ICE Participant List/Role***

Chris Cox	NOAA-PSD/CIRES	christopher.j.cox@noaa.gov	Project Lead, deployment, Alert/Eureka contact
Sara Crepinsek	NOAA-PSD/CIRES	sara.crepinsek@noaa.gov	Project Lead, deployment, implementation
Chuck Long	NOAA-GMD/CIRES	chuck.long@noaa.gov	Experiment Consultant
Allison McComiskey	NOAA-GMD	allison.mccomiskey@noaa.gov	Logistics: GMD
Taneil Uttal	NOAA-PSD	taneil.uttal@noaa.gov	Logistics: PSD
Jim Wendell	NOAA-GMD	jim.wendell@noaa.gov	Engineering Support
Emiel Hall	NOAA-GMD/CIRES	emiell.hall@noaa.gov	NOAA calibrations, deployment
Brian Vasel	NOAA-GMD	brian.vasel@noaa.gov	GMD/Barrow station logistics
Bernd Loose	AWI	Bernd.Loose@awi.de	AWI, engineering
Holger Schmithüsen	AWI	Holger.Schmithuesen@awi.de	AWI, main contact
Gert König-Langlo	AWI	gert.koenig-langlo@awi.de	AWI BSRN contact, retiring
Jörgen Konings	Hukseflux	jorgen@hukseflux.com	providing Hukseflux designs
Matt Martinsen	NOAA-GMD	matthew.martinsen@noaa.gov	BRW observatory
Bryan Thomas	NOAA-GMD	bryan.thomas@noaa.gov	BRW observatory, station chief
Ursula Weisser	ZAMG	ursula.weiser@zamg.ac.at	CCIWG Sonnblick contact (modified Eigenbrodt)
Tom Kirk	Eppley	tomkirk@eppleylab.com	Eppley industry contact. Can loan instruments.
Julian Groebner	PMOD	julian.groebner@pmodwrc.ch	PMOD ventilation
Matthew Shupe	NOAA-PSD/CIRES	matthew.shupe@noaa.gov	Experiment Consultant
Ola Persson	NOAA-PSD/CIRES	ola.persson@noaa.gov	Experiment Consultant
Steven Semmer	NCAR	semmer@ucar.edu	Persson/Semmer spray system
Victor Cassella	Kipp&Zonen	Victor.Cassella@kipponen.com	CMP22, CGR4, 2 CVF4 ventilation systems
Dick Jenkins	DeltaT	dick.jenkins@delta-t.co.uk	SPN1
Laurent Vuilleumier	Meteoswiss	laurent.vuilleumier@meteoswiss.ch	Ventilation and heating system loan used at Jungfraujoch
William Beuttell	EKO	beuttell@eko-usa.com	EKO main contact